Author's Accepted Manuscript

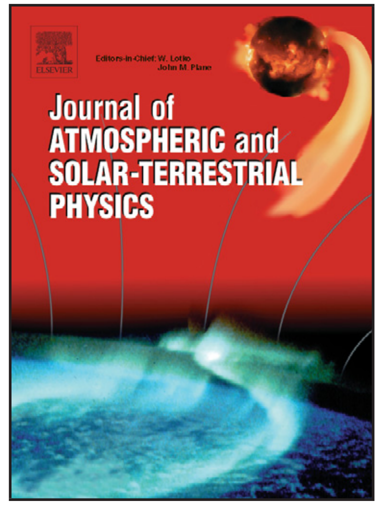

www.elsevier.com/locate/jastp

Analysis of large scale MHD quantities in expanding magnetic clouds

María Soledad Nakwacki, Sergio Dasso, Cristina Hemilse Mandrini, Pascal Démoulin

PII: S1364-6826(08)00073-4
DOI: doi:10.1016/j.jastp.2008.03.006
Reference: ATP 2689

Journal of Atmospheric and Solar–Terrestrial Physics

Received date: 4 May 2007
Revised date: 27 February 2008
Accepted date: 23 March 2008

Cite this article as: María Soledad Nakwacki, Sergio Dasso, Cristina Hemilse Mandrini and Pascal Démoulin, Analysis of large scale MHD quantities in expanding magnetic clouds, *Journal of Atmospheric and Solar–Terrestrial Physics* (2008), doi:10.1016/j.jastp.2008.03.006

Analysis of large scale MHD quantities in expanding magnetic clouds

María Soledad Nakwacki [a,*] Sergio Dasso [a,b,1]
Cristina Hemilse Mandrini [a,1], Pascal Démoulin [c]

[a] *Instituto de Astronomía y Física del Espacio, CONICET-UBA, CC. 67 Suc. 28, 1428 Buenos Aires, Argentina*

[b] *Departamento de Física, FCEN, UBA, Argentina*

[c] *Laboratoire d'Etudes Spatiales et d'Instrumentation en Astrophysique, LESIA, Observatoire de Paris, 5 place Jules Janssen, F-92195 Meudon Cedex, France*

Abstract

Magnetic clouds (MCs) transport the magnetic flux and helicity released by the Sun. They are generally modeled as a static flux rope traveling in the solar wind, though they can present signatures of expansion. We analyze three expanding MCs using a self-similar free radial expansion model with a cylindrical linear force-free field (i.e. Lundquist solution) as the initial condition. We derive expressions for the magnetic fluxes, the magnetic helicity and the magnetic energy per unit length along the flux tube. We find that these quantities do not differ more than 25% when using the static or expansion model.

Key words: Interplanetary magnetic fields, Ejecta, driver gases, and magnetic clouds

PACS: 96.50.Bh, 96.50.Uv

---

1 Introduction

Solar activity sometimes involves transient releases of magnetized plasma into the interplanetary medium. This material can be observed in situ as a magnetic cloud (MC). MCs are large scale magnetic flux ropes. They are a subset of interplanetary coronal mass ejections (ICMEs) and carry a large amount of magnetic helicity, magnetic flux and energy away from the Sun. The main characteristics of these structures have been enumerated by Burlaga and Klein (1980): (i) an enhanced magnetic field intensity when compared with its surroundings, (ii) a smooth and large rotation of the magnetic field vector along the observing time period, and (iii) a low proton temperature.

In general, MCs have been considered as rigid flux ropes that travel through the interplanetary medium. In particular, their magnetic field have been frequently modeled using the Lundquist's model

(Lundquist, 1950), which considers a static and axially-symmetric linear force-free magnetic configuration (see, e.g., Goldstein, 1983; Burlaga, 1988; Lepping et al., 1990; Burlaga, 1995; Lynch et al., 2003). However, there exist many other models that can be used to describe the magnetic structure of MCs. A not evolving cylindrical shape for the cloud section and a non-linear force-free field was considered by Farrugia et al. (1999); while Mulligan et al. (1999), Hidalgo et al. (2002), and Cid et al. (2002) supposed a cylindrical cloud but a non-force free field. Hu and Sonnerup (2001), and Vandas and Romashets (2002) applied non cylindrical static models to MCs.

However, some MCs present a significantly larger velocity in their front part than in their back region. This characteristic shows that the MC is in expan-

* Corresponding author, e-mail: sole@iafe.uba.ar. Fellow of CONICET, Argentina.
[1] Member of the Carrera del Investigador Científico, CONICET, Argentina

sion. In these cases static models are not able to reproduce closely the observed magnetic field profiles; so, several dynamical models have been developed to describe these clouds during their observation time. Some of them describe the cloud cross-section as a circle considering only a radial expansion (see, e.g., Farrugia et al., 1993; Osherovich et al., 1993a; Farrugia et al., 1997), or include expansion in both directions, radial and axial (see, e.g., Shimazu and Vandas, 2002; Berdichevsky et al., 2003). There are also dynamical models for which the cloud has an expanding elliptical shape (Hidalgo, 2003). The main aim of these models is to take into account the time evolution of the magnetic field as the spacecraft crosses the cloud including the effect that expansion may have on the correct interpretation of the observations. In this way, a better determination of the global MC shape and its physical parameters can be found.

One aspect worth to quantify in these structures are the global magnetohydrodynamic (MHD) quantities, such as magnetic flux, magnetic helicity, and energy, which are of significant interest to link coronal mass ejections to their interplanetary counterparts. These quantities have been computed and compared using different models (the classical Lundquist's and other cylindrical static models mentioned above) by Dasso et al. (2005b), considering a new model independent method for non-expanding MCs by Dasso et al. (2006) and for expanding MCs by Dasso et al. (2007). A comparison of different techniques applied to fit different models has been done analyzing the output of numerical simulations by Riley et al. (2004).

In this paper we analyze examples for which, due to either the cloud orientation or the behavior of the velocity profile, we have to take into account the effects of the expansion in the radial direction. We derive expressions for the global MHD quantities, assuming a self-similar expansion in the radial component (in the cloud coordinates, see Sec. 3.1) of the field and a cylindrical symmetry. We also derive these quantities using the classical static Lundquist's model. The three MCs presented in this work were observed from 1998 to 2001. These have been selected from the full set of clouds observed during that period ($\sim$ 40) because their magnetic field shows well-defined cloud characteristics, and present the strongest radial expansion with meaningless expansion in the axial direction. This paper is organized as follows. In Section 2, we present a brief description of the classical static Lundquist's model and, in detail, a radial self-similar expansion model and deduce the corresponding equations for global MHD quantities. In Section 3, we describe our data analysis method; while in Section 4, we present the observations and our results for the different clouds and both models, static and expansion. Finally, in Section 5 we discuss our results and conclude.

2 Static and expansion models

2.1 Lundquist model

Lundquist model (Lundquist, 1950) considers that: (a) the magnetic forces are dominant against the pressure gradient, with magnetic pressure balanced by magnetic tension, so that $\vec{J} \times \vec{B} = 0$ (force free field, $\vec{J} // \vec{B}$, where $\vec{J}$ and $\vec{B}$ are the current density and magnetic field vectors, respectively), (b) cylindrical symmetry, and (c) the ratio between current and the magnetic field intensity is uniform (linear force free). Thus, the cylindrical components of the magnetic field are:

$$B_r = 0 \quad (1)$$

$$B_\phi = B_0 J_1(\alpha r) \quad (2)$$

$$B_z = B_0 J_0(\alpha r) \quad (3)$$

In these equations J_n are the Bessel functions of the first kind of order n with n being natural, α is a constant that represents the ratio between the current and $|\vec{B}|$ ($\alpha/2$ quantifies the twist of the field lines near the cloud center). B_0 is the strength of the magnetic field at the cloud axis, and r is the radial distance to the axis of the cylinder. We will call model S to this model.

Using Eqs. 1-3, the expressions for the magnetic flux across the plane perpendicular to the cloud axis (Φ_z), across the surface defined by the cloud axis and the radial direction (Φ_ϕ), the relative magnetic helicity (H_r), and the magnetic energy (E_m) can be derived (see e.g. Dasso et al. (2003, 2005b); Nakwacki et al. (2005)):

$$\Phi_z = \frac{2\pi}{\alpha} R B_0 J_1(\alpha R) \quad (4)$$

$$\frac{\Phi_\phi}{L} = \frac{B_0}{\alpha}[1 - J_0(\alpha R)] \quad (5)$$

$$\frac{H_r}{L} = \frac{2\pi}{\alpha} B_0^2 R^2 [J_1^2(\alpha R) - J_0(\alpha R) J_2(\alpha R)] \quad (6)$$

$$\frac{E_m}{L} = \frac{B_0^2 R^2}{8}[2J_1^2(\alpha R) - J_0(\alpha R) J_2(\alpha R) + J_0^2(\alpha R)] \quad (7)$$

In these equations R is the cloud radius and the last three quantities are computed per unit length (L).

2.2 Free radial self-similar expansion

We summarize the basic equations for the self-similar expansion model used by Osherovich et al. (1993b) and Farrugia et al. (1993) and we derive the global MHD quantities (Φ_z, Φ_ϕ/L, H_r/L, and E_m/L). This model partially explains the asymmetry observed in the magnetic field of clouds that present a significant radial expansion, while traversed by the spacecraft. This model considers: (a) the continuity equation, (b) the inertial term in the Navier-Stokes equation equal to zero (i.e. no forces are applied to any element of fluid), and (c) the ideal induction equation, all of them in cylindrical symmetry, allowing only a dependence on r and t (i.e. any quantity M can be written as $M = M(r,t)$). The system of equations is:

$$\partial_t \rho + \frac{1}{r}\partial_r(r\rho V_r) = 0 \tag{8}$$

$$\partial_t V_r + \frac{1}{r}(V_r\partial_r)V_r = 0 \tag{9}$$

$$\partial_t A_r = 0 \tag{10}$$

$$\partial_t A_z = -\frac{V_r}{r}\partial_r(rA_\phi) \tag{11}$$

$$\partial_t A_\phi = -V_r\partial_r(A_z) \tag{12}$$

where ρ is the mass density, V_r is the plasma radial velocity, and A_r, A_ϕ, and A_z are the components of $\vec{A}$ which is the vector potential ($\vec{B} = \vec{\nabla} \times \vec{A}$), and, in this case, depends only on r and t ($\vec{A}(r,t)$).

The dependence of the relevant physical quantities on r and t is assumed to be self-similar; so, r and t are combined in $\eta = r/\xi(t)$, where $\xi(t)$ is a function depending on the forces applied on the system. From Eq. 8, we obtain $V_r(r,t) = \frac{r\xi'(t)}{\xi(t)}$. Replacing this expression for the velocity in Eq. 9, we get $\xi(t) \propto t$ (free radial expansion). Thus, the temporal evolution of the radial component of the velocity field can be written as:

$$V_r(r,t) = \frac{r}{T(1+t/T)} \tag{13}$$

where T can be interpreted as the cloud age (i.e. the duration of the selfsimilar expansion prior to the start of Wind observations at 1 AU (see Farrugia et al., 1993)).

From the velocity evolution, we obtain the time evolution for the cloud radius (size), which increases with t as:

$$R(t) = R^* \frac{1 + t/T}{1 + t^*/T}, \tag{14}$$

where R^* is the cloud radius at a given reference time $t = t^*$.

To find the magnetic field configuration under these conditions, we use Eqs. 11-12 imposing that the magnetic fluxes also depend on the self-similar variable. Once this is done, we write the magnetic field components in terms of the magnetic fluxes and assume that at some time ($\hat{t}$) the magnetic field is linear force-free. However, this configuration can change with time, according with the temporal evolution implied from the dependence with η. With all these considerations, the magnetic field can be written as:

$$B_r = 0, \tag{15}$$

$$B_\phi(r,t) = B_0^\phi(t) J_1(\alpha(t) r), \tag{16}$$

$$B_z(r,t) = B_0^z(t) J_0(\alpha(t) r), \tag{17}$$

where $B_0^z(t) = \hat{B}_0 \frac{(1+\hat{t}/T)^2}{(1+t/T)^2}$, $B_0^\phi(t) = \hat{B}_0 \frac{1+\hat{t}/T}{1+t/T}$, and $\alpha(t) = \hat{\alpha} \frac{1+\hat{t}/T}{1+t/T}$, with $\hat{B}_0$ and $\hat{\alpha}$ constants. We will call model E to this model.

From Eqs. 15-17 we derive expressions for the relative magnetic helicity per unit length, the fluxes, and the magnetic energy per unit length:

$$\Phi_z = \frac{2\pi}{\hat{\alpha}} \hat{R} \hat{B}_0 J_1(\hat{\alpha}\hat{R}) \tag{18}$$

$$\frac{\Phi_\phi}{L} = \frac{\hat{B}_0}{\hat{\alpha}}[1 - J_0(\hat{\alpha}\hat{R})] \quad (19)$$

$$\frac{H_r}{L} = \frac{2\pi}{\hat{\alpha}}\hat{B}_0^2\hat{R}^2[J_1^2(\hat{\alpha}\hat{R}) - J_0(\hat{\alpha}\hat{R})J_2(\hat{\alpha}\hat{R})] \quad (20)$$

$$\frac{E_m}{L} = \frac{\hat{B}_0^2\hat{R}^2}{8}[(1 + \frac{(1+\frac{\hat{t}}{T})}{(1+\frac{t}{T})})J_1^2(\hat{\alpha}\hat{R}) - J_0(\hat{\alpha}\hat{R})J_2(\hat{\alpha}\hat{R}) + \frac{(1+\frac{\hat{t}}{T})}{(1+\frac{t}{T})}J_0^2(\hat{\alpha}\hat{R})] \quad (21)$$

where $\hat{R}$ is the radius of the cloud at $\hat{t}$. From the previous Eqs. we see that Φ_z, Φ_ϕ/L and H_r/L are constant with time. The expansion produces an increment on $R(t)$, which cancels the decay of $B_0^{\phi,z}(t)$ and $\alpha(t)$. On the other hand, the magnetic energy per unit length (Eq. 21) depends on time. Note that in $t = \hat{t}$ the expression for E_m/L is the same as for the Lundquist magnetic configuration (Eq. 7).

3 Data analysis

3.1 Method of analysis

The magnetic field observations we analyze here are in GSE (Geocentric Solar Ecliptic) coordinates. In this right-handed system of coordinates, $\hat{x}_{GSE}$ corresponds to the Earth-Sun direction, $\hat{z}_{GSE}$ points to the North (perpendicular to the ecliptic plane) and $\hat{y}_{GSE}$ is in the ecliptic plane and points to the dusk when an observer is near Earth (thus, opposing to the planetary motion).

To understand the cloud properties it is convenient to define a local system of coordinates linked to the cloud (i.e., the cloud frame). In this system $\hat{z}_{\text{cloud}}$ is along $\vec{B}$, such that $\hat{z}_{\text{cloud}}.\vec{B} > 0$ at the cloud axis. Since the speed of the cloud is mainly in the Sun-Earth direction and is much larger than the spacecraft speed, which can be supposed to be at rest during the cloud observing time, we assume a rectilinear spacecraft trajectory in the cloud frame. The trajectory defines a direction $\hat{d}$; so, we take $\hat{y}_{\text{cloud}}$ in the direction $\hat{z}_{\text{cloud}} \times \hat{d}$ and $\hat{x}_{\text{cloud}}$ to complete the right-handed orthonormal base $(\hat{x}_{\text{cloud}}, \hat{y}_{\text{cloud}}, \hat{z}_{\text{cloud}})$. Thus, $B_{x,\text{cloud}}$, $B_{y,\text{cloud}}$, $B_{z,\text{cloud}}$ are the components of $\vec{B}$ in this new base.

The cloud frame is especially useful when the impact parameter, p (the minimum distance from the spacecraft to the cloud axis), is small compared to the MC radius. In particular, for $p = 0$ and a MC described using a cylindrical magnetic configuration, $\vec{B}(r) = B_z(r)\hat{z} + B_\phi(r)\hat{\phi}$, we have $\hat{x}_{\text{cloud}} = \hat{r}$ and $\hat{y}_{\text{cloud}} = \hat{\phi}$ when the spacecraft leaves the cloud.

In this case, the magnetic field data obtained by the spacecraft will show: $B_{x,\text{cloud}} = 0$, a large and coherent variation of $B_{y,\text{cloud}}$ (with a change of sign), and an intermediate and coherent variation of $B_{z,\text{cloud}}$, from low values at one cloud edge, taking the largest value at its axis and returning to low values at the other edge.

We also define the latitude angle (θ) between the ecliptic plane and the cloud axis, as well as the longitude angle (ϕ) between the projection of the axis on the ecliptic plane and the Earth-Sun direction ($\hat{x}_{GSE}$), measured counterclockwise (see Figure 1). These angles will give the cloud orientation. The minimum variance (MV) method (Sonnerup and Cahill, 1967) has been used to estimate the orientation of MCs (see e.g., Bothmer and Schwenn, 1998; Lepping et al., 1990; Farrugia et al., 1999; Dasso et al., 2003; Gulisano et al., 2005). It provides a good estimation of the MC orientation if p is small compared to R and if the in/out bound magnetic fields are not significantly asymmetric. For ideal static cylindrical Lundquist's MCs (linear force free field), a quantification (in function of p) of the differences between the real direction of the cloud axis and that obtained using the MV method (Gulisano et al., 2007). Moreover, when a cloud presents a strong expansion, the directions found with the MV method will mix two different effects in the variance of the field: (1) the effect of the coherent rotation of $\vec{B}$ (which provides the cloud orientation) and (2) the effect of the cloud 'aging' (the decrease of the field strength with time due to magnetic flux conservation combined with cloud expansion). This latter effect is not associated with the cloud orientation; thus, we apply the MV technique to the normalized field, $\vec{B}(t)/|\vec{B}(t)|$, to decrease the influence of cloud 'aging'. Once we determine θ and ϕ, we construct a rotation matrix from the GSE to the cloud system and we obtain the components of the observed magnetic field in the cloud coordinates: $B_{x,\mathrm{cloud}}$, $B_{y,\mathrm{cloud}}$, $B_{z,\mathrm{cloud}}$.

3.2 Fitting method

After finding the orientation of the cloud, we fit models for the velocity and the magnetic field observed profiles to obtain the parameters that better describe the clouds under these models. These parameters will be also used to calculate the relevant MHD quantities. Next sections give an explanation of both fitting (velocity and magnetic field).

3.2.1 Fitting the velocity profile

The speed of the spacecraft can be considered as constant in the frame of the MC center of mass; in this way, we can give an estimation of the spacecraft position as $r_{sat} = U(t - t_c)$, where t_c (center time) is the time at which the spacecraft crosses the cloud center, and U is the bulk velocity of the cloud. We can define $\delta = t_f - t_0$ as the observational range of time, with t_0 the cloud start time and t_f the cloud end time.

For the static case, we can give an estimation of t_c as $t_c = \delta/2 + t_0$ coinciding with the center of the structure. With these considerations the radial position r_{sat} is defined such that $r_{sat} < 0$ before the spacecraft crosses the cloud axis and $r_{sat} > 0$ after crossing it.

For MCs in expansion, t_c will not necessarily coincide with the central crossing time, due to the asymmetry given by the expansion. In this case, we find $t_c = 2t_f/(1 + t_f/T)$. This expression can be obtained using r_{sat} and the Eq. 14 (both measured from T, which is used as the reference time ($t_0 = T$)) evaluated in T ($r_{sat}(T) = R_T$) and in t_f ($r_{sat}(t_f) = R_f$). In this way, we can write $t_f = T + \delta$. Then, we replace t_c in Eq. 13 measured from T, where we have used that $r = r_{sat}$. The total velocity is the expansion plus the translation velocity, represented by U:

$$V_{x,cloud}(t) = U + U[\frac{\frac{T+\delta}{T+t}}{1 + \frac{\delta}{2T}}] \tag{22}$$

To make an additional simplification we assume that the bulk velocity U can be estimated as $U \sim < V_{x,cloud} >$, $< V_{x,cloud} >$ being the mean value of speed during the observing time. Then, the observed $V_{x,cloud}(t)$ can be model by:

$$V_{x,cloud}(t) = < V_{x,cloud} > + < V_{x,cloud} > [\frac{\frac{T+\delta}{T+t}}{1 + \frac{\delta}{2T}}] \tag{23}$$

We compare observations of $V_{x,cloud}$ with Eq. 23, and fit this model to the data using the "fminunc" routine of Matlab (version 6.5 R13) to find the free parameter T.

3.2.2 Fitting the magnetic profile

The free parameters $\{B_0, \alpha\}$ for the Lundquist's model, and $\{\hat{B}_0, \hat{\alpha}, \hat{t}\}$ for the expansion model are fitted to the observations of the magnetic field components $B_{y,cloud}$ and $B_{z,cloud}$ using the same nonlinear fitting routine as for T. The theoretical expressions for the components of the magnetic field are given by Eqs. 2-3 for model S and by Eqs. 16-17 for model E. It is important to notice that in both cases, S and E, the free parameters are fitted such that, $B_{z,cloud}(r = R)$ is not necessarily zero.

4 Observations and results

4.1 The observations

We study three MCs observed from 1998 to 2001 that belong to an extended set of $\sim$ 40 MCs identified in this period by R. Lepping (http://lepmfi.gsfc.nasa.gov-/mfi/mag_cloud/pub1.html). The number identifying the cloud and the start and end times are shown in the first 3 columns of Table 1. These clouds were selected because of their well-behaved magnetic profiles, their velocity profiles showing expansion and their low proton β parameter, β_p (i.e., the ratio between the proton pressure and the magnetic pressure), as expected from the two commonly observed signatures in MC: low proton temperature and high $|\vec{B}|$.

We analyze in situ measurements of the magnetic field components in GSE obtained by the Magnetic Field Instrument (MFI, Lepping et al. (1995)) and plasma data obtained by the Solar Wind Experiment (SWE, Ogilvie et al. (1995)), both aboard Wind. The temporal cadence of MFI data is 3 seconds, while for SWE it is 100 seconds. We set the boundaries of the clouds using the information available in Lepping's cloud identification web page (see Table 1). The orientation angles of the cloud axis, θ and ϕ, are given in the fourth and sixth columns of Table 1. We compare our angles with those informed by R. Lepping in http://lepmfi.gsfc.nasa.gov/mfi/mag_cloud_S1.html, the latter are include in the fifth and seventh columns of Table 1. For clouds 1 and 3 the difference with Lepping's angles (for both θ and ϕ) is less than 19°; but for cloud 2 the difference in ϕ is $\sim 35°$, while θ takes the same value. The previous webpage also reports an estimation for p/R (included in the last column of Table 1), which is less than 15% for cloud 1 and 3 and less than 26% for cloud 2. Thus, because the spacecraft is crossing close to the axis of the clouds, it is a good assumption to consider $p \ll R$. It is noteworthy that the angles obtained with the normalized MV method differ by less than 7° from those obtained with a non-normalized MV.

We analyze β_p OMNI data with a temporal cadence of 1 minute (for further information see http://omniweb.gsfc.nasa.gov/html/ow_data.html). Lepping et al. (2003) determined the typical values for parameters characterizing MCs, they concluded that $\beta_p \ll 1$, being its typical value ~ 0.12. The value of $< \beta_p >$ (i.e. mean value of β_p during the MCs observation time) is shown in Table 1 for each cloud. The three MCs analyzed here have $\beta_p < 0.08$, which is below the typical one reported by Lepping et al. (2003).

The profiles of the dimensionless parameter β_p are shown in Figure 2. From these figures we can see that in the three events a sudden change of β_p (from the higher values typical in solar wind to the lower ones typical in MCs) clearly marks the beginning of the clouds; but we want to emphasize that after the end boundaries (selected by R. Lepping from the observed magnetic behavior), the values of β_p do not return to the typical solar wind values for cloud 3, while they do for MCs 1 and 2. In this region β_p remains being low. This signature, beyond the trailing edge of the MC, is consistent with the observation of a structure which originally was part of the rear of a previous larger closed flux rope, as discussed by Dasso et al. (2006) for a different MC. In the example studied in Dasso et al. (2006), those authors proposed that magnetic flux was earlier removed from the cloud front due to magnetic reconnection between the MC front and its environment; however, magnetic flux at the rear was not removed and it still remained there at 1AU. Thus, a back region presenting β_p values typical of MCs are observed after the flux rope, as in the clouds studied here.

4.2 Velocity results

From the fitted T (described in Sec. 3.2.1), we calculate the initial radius (R_0, when Wind enters the cloud) and the final radius (R_f, when Wind leaves the cloud). To compare these values with the static case, we also compute the static radius R_s as one half of the total distance traveled by Wind through the MC, considering a constant speed equal to $< V_{x,cloud} >$.

Figure 3 shows the three velocity profiles, a variation of less than 100 km/s is present between the start time and the end time for the three clouds. The MC labeled as 1 presents the largest fluctuations, while MC 3 the smallest one and the best fitting.

Table 2 shows the fitted parameter T, $< V_{x,cloud} >$, and the radii for the three clouds. The first cloud is the oldest and slowest, and the last is the youngest and fastest. For the three MCs, R_s is between R_0 and R_f and the values are similar.

4.3 Magnetic field results

Figure 4 shows the observations and models for the magnetic field profiles; the dots correspond to the observations, the thin full lines to model E, and the thick dashed lines to model S. We show (vertical thin dashed lines) the cloud boundaries and also the cloud center time, as deduced from model E (i.e., the time at which the spacecraft crosses the cloud axis). These times are 01:38 UT on August 21, 1998, for cloud 1, 00:20 UT on August 10, 1999, for cloud 2, and 12:12 UT on April 22, 2001, for cloud 3.

In Table 3 we report the parameters obtained from the fitting, as well as $\chi^2 =< (\vec{B}^{obs} - \vec{B}^{fit})^2 >$, where 'obs' and 'fit' correspond to the observations and the fitting, respectively. Note that the condition $\alpha R \sim 2.4048$ is valid for the static case and also for the expansion model. However, in the later model, α and R depend on t, so from the expressions given in Sec. 2.2 we obtain $\alpha(t)R(t) = \hat{\alpha}R_o(1+\hat{t}/T)$, where $\hat{t}$ is fitted to the data. Whether this condition is satisfied or not can be seen computing the expression given above. Clearly, for model S we obtain that αR_s is in the range $[2-2.8]$, and for model E this range is: $[1.8-2.6]$.

The values of χ^2 are proxies for the quality of the fitting. Cloud number 3 (April, 2001) shows the best quality fitting for model E, in agreement with the best fitting for the bulk velocity (right panel of Figure 3).

From Figure 4 we can see that, as shown in Table 3, the best fitting is found for model E (both models give similar values of χ^2 for cloud 2).

The observed decay of the azimuthal field component, $1-|B^{obs}_{y,cloud}(t_f)|/|B^{obs}_{y,cloud}(t_0)|$, turns out to be 46%, 29%, and 22% for clouds 1, 2 and 3, respectively. For model E, this component is expected to decay as $1-|B^{fit}_{y,cloud}(t_f)|/|B^{fit}_{y,cloud}(t_0)|$, which corresponds to 13%, 12%, and 14%, which is significantly lower than the observed decay. This indicates that the observed asymmetry is not only due to the cloud expansion but also due to spatial asymmetries. Of course, the prediction of model S is that $|B_{y,cloud}(t)|$ will be the same at the cloud start and end.

4.4 *Computing MHD global invariants*

From Eqs. (4-7) and (18-21) and the fitted parameters for models S and E (see Tables 2-3), we compute the cloud global MHD quantities. Table 4 shows the results.

For the fluxes and the magnetic helicity we compute the relative difference between the values obtained with both models ($\Delta = \frac{S-E}{<S,E>}$, where $<S,E>= (S+E)/2$). Considering the three studied MCs, we find that, the axial magnetic flux Φ_z is in the range $[0.13-0.26]$nTAU^2 and changing the model it varies in less than 14%. Similarly, the azimuthal magnetic flux per unit length Φ_ϕ/L is in the range $[0.45-0.90]$nTAU and varies in less than 25%. We have also found that the magnetic helicities per unit length H_r/L are in the range $[0.11-0.18]$nT^{2}AU^3 with a variation of less than 17%. The ranges for the three quantities were obtained considering both models, static and expansion.

For the magnetic energy we perform a different comparison between both models because model E predicts a decay, while S does not. We compute Δ between the initial and final values for model E and we find that the magnetic energy decay is less than 12% during the observed range of time. We also compare the magnetic energy values (E_m) between both models, computing now $\Delta = (S - E_{av})/ < S, E_{av} >$, where E_{av} is the average value of E_m for model

E (averaging its start and final values). For clouds number 2 and 3, we obtain $\Delta \lesssim 15\%$, while for cloud 1 we find that $\Delta \sim 25\%$. The range for this quantity is $[0.10 - 0.20]\mathrm{nT}^2\mathrm{AU}^2$.

5 Summary, discussion and conclusions

We have studied three magnetic clouds (MCs) observed by Wind between 1998 and 2001, which showed signatures of significant expansion and a well behaved magnetic field. The main aim of our study is to quantify MHD global quantities in these examples using an expansion model. Then, to compare the later values to those derived from the more generally used static model (Lundquist model) in order to evaluate the uncertainty in the results found when using static models. One of the reasons to improve the estimation of magnetic fluxes and helicity in MCs is that these quantities can be used to link solar phenomena with their manifestations in the interplanetary medium, since they are conserved both in the solar atmosphere and in the heliosphere. In particular, Mandrini et al. (2005b) and Luoni et al. (2005) compared the coronal magnetic helicity released from a very small and a typical AR with the helicity content of the associated MCs. They found a very good agreement between the coronal and interplanetary values for both events. The difference between the small and large events was around 3 orders of magnitude.

We set the boundaries of the three studied MCs as those selected by R. Lepping. Finding the boundaries for some MCs is an open issue (e.g., Russell and Shinde, 2005; Wimmer-Schweingruber et al., 2006). For the three cases studied here, we observe a sudden change of β_p, from high values (typical of the solar wind) to low values (typical of MCs), in agreement with the times set for the cloud start time. However, a low value of β_p still remains beyond the cloud end times selected considering the behavior of the magnetic field components. As suggested by Dasso et al. (2006), the existence of cloud properties beyond the selected end time (beyond the rear part chosen for the cloud) can be a indirect signature of its interaction (via magnetic reconnection) with the front surrounding solar wind, which removed magnetic flux from the front of the previously larger original flux rope. This kind of interaction allows that part of the outer larger original flux rope still remains in the back of the MC.

The two models used for the analysis are based on Lundquist's solution. As mentioned above, one is the classical static solution and the second one includes a self-similar radial expansion. The expansion rate is obtained fitting the model to the observed plasma velocity. We derive expressions for the magnetic fluxes, helicity, and energy, for the expansion model, we quantify these values using parameters coming from a fitting to the observations, and, finally, we compare these values to those coming from the classical static model.

We have found that, assuming a cloud length of $\sim$ 1AU, the azimuthal flux (Φ_ϕ) is larger than the axial flux (Φ_z); in particular Φ_ϕ is always at least a factor of 2 larger than Φ_z for the three MCs and the two models studied here. In the extreme case (model E for the cloud 1 on August, 1998) Φ_ϕ is almost one order of magnitude larger than Φ_z. Similar results were found by Mandrini et al. (2005b) and Attrill et al. (2006) who computed the magnetic flux in the two dimming regions associated with two eruptions (see also, Webb et al., 2000). In both works it was found that the flux in the dimmings was comparable mainly to the flux in the azimuthal component of the MC (when assuming a length compatible with both solar and interplanetary observations). These results led these authors to propose that the ejected flux rope is formed by successive reconnections in a sheared arcade during the eruption process (see also, Mandrini et al., 2005a).

The three events analyzed have cloud typical sizes (R $\sim$ 0.1 AU), but smaller values for the magnetic axial field ($B_0 \sim$ 10 nT) than those typically observed at 1AU ($B_0 \sim 20$ nT) (see, Lepping et al., 2003). The range of values found for the helicity (see Sec. 4.4) is equivalent to [5.6-9.1]$\times 10^{41}$Mx^2/AU, and is in agreement with the range obtained from an statistical study (using Lundquist's model) by van Driel-Gesztelyi et al. (2003). These authors found a mean value for $H_r/L = 4 \times 10^{42}$Mx^2/AU, larger than the values obtained here but with a spread of more than 3 orders of magnitude. On the other hand, quantifications of H_r/L comparing different static models to describe different magnetic configurations in MCs were done by Gulisano et al. (2005) and Dasso et al. (2005a). It was found that the differences in H_r/L when changing from static model was much smaller than when changing from event. For the cloud set studied by these later authors, H_r/L stayed in the range $\sim 10^{41} - 10^{43}$Mx^2/AU; the range of H_r/L presented here agrees with these two studies.

As in Gulisano et al. (2005) and Dasso et al. (2005a), we have also found that the difference of H_r/L when changing models (but in this work comparing an static and an expansion model) is smaller than the difference when the cloud is changed (see Table 4). This also is true for the axial magnetic flux (Dasso et al., 2005a) and for the azimuthal magnetic flux per unit length (comparing the results obtained by Attrill et al. (2006) and those in Dasso et al. (2006) which differ in almost a factor 3). Thus, we conclude that H_r/L, Φ_z, and Φ_ϕ/L, can be obtained as a first order approximation using a simple static model, since considering the radial expansion effect will not affect strongly their values. Finally, all the previous results suggest that these global MHD quantities are well determined in clouds, even in those showing strong expansion.

Acknowledgments: This research has made use of NASA's Space Physics Data Facility (SPDF). C.H.M. and P.D. acknowledge financial support from CNRS (France) and CONICET (Argentina) through their cooperative science program (N^0 20326). This work was partially supported by the Argentinean grants: UBACyT X329, PIP 6220 (CONICET), and PICT N^0 05-33370. S.D. and C.H.M. are members of the Carrera del Investigador Científico, CONICET. M.S.N. is a fellow of CONICET.

References

Attrill, G., Nakwacki, M. S., Harra, L. K., van Driel-Gesztelyi, L., Mandrini, C. H., Dasso, S., Wang, J., 2006. Using the Evolution of Coronal Dimming Regions to Probe the Global Magnetic Field Topology. Solar Phys., 238, 117–139.

Berdichevsky, D. B., Lepping, R. P., Farrugia, C. J., 2003. Geometric considerations of the evolution of magnetic flux ropes. Physical Rev. E, 67 (3), 036405.1–036405.8.

Bothmer, V., Schwenn, R., 1998. The structure and origin of magnetic clouds in the solar wind. *Ann. Geophys.* 16, 1–24.

Burlaga, L. F., Jul. 1988. Magnetic clouds and force-free fields with constant alpha. Journal of Geophys. Res., 93, 7217–7224.

Burlaga, L. F., 1995. Interplanetary magnetohydrodynamics. New York : Oxford University Press, 1995.

Burlaga, L. F., Klein, L., 1980. Magnetic clouds in the solar wind. *NASA STI/Recon Technical Report N* 80, 22221.

Cid, C., Hidalgo, M. A., Nieves-Chinchilla, T., Sequeiros, J., Viñas, A. F., 2002. Plasma and Magnetic Field Inside Magnetic Clouds: a Global Study.

Solar Phys., 207, 187–198.

Dasso, S., Mandrini, C. H., Démoulin, P., Farrugia, C. J., 2003. Magnetic helicity analysis of an interplanetary twisted flux tube. Journal of Geophys. Res., 108 (A10), 1362–1369.

Dasso, S., Gulisano, A. M., Mandrini, C. H., Démoulin, P., 2005a. Model-independent large-scale magnetohydrodynamic quantities in magnetic clouds. Adv. in Space Res., 35, 2172–2177.

Dasso, S., Mandrini, C. H., Démoulin, P., Luoni, M. L., Gulisano, A. M., 2005b. Large scale MHD properties of interplanetary magnetic clouds. Adv. in Space Res., 35, 711–724.

Dasso, S., Mandrini, C. H., Démoulin, P., Luoni, M. L., 2006. A new model-independent method to compute magnetic helicity in magnetic clouds. Astron. Astrophys., 455, 349–359.

Dasso, S., Nakwacki, M. S., Démoulin, P., Mandrini, C. H., 2007. Progressive transformation of a flux rope to an ICME. Solar Phys., 244, 1-2, 115–137.

Farrugia, C. J., Burlaga, L. F., Osherovich, V. A., Richardson, I. G., Freeman, M. P., Lepping, R. P., Lazarus, A. J., 1993. A study of an expanding interplanetary magnetic cloud and its interaction with the earth's magnetosphere - The interplanetary aspect. Journal of Geophys. Res., 98, 7621–7632.

Farrugia, C. J., Osherovich, V. A., Burlaga, L. F., 1997. The non-linear evolution of magnetic flux ropes: 3. effects of dissipation . *Ann. Geophys.*, 152–164.

Farrugia, C. J., Janoo, L. A., Torbert, R. B., Quinn, J. M., Ogilvie, K. W., Lepping, R. P., Fitzenreiter, R. J., Steinberg, J. T., Lazarus, A. J., Lin, R. P., Larson, D., Dasso, S., Gratton, F. T., Lin, Y., Berdichevsky, D., 1999. A Uniform-Twist Magnetic Flux Rope in the Solar Wind. In: AIP

Conf. Proc. 471: Solar Wind Nine. pp. 745–748.

Goldstein, H., Nov. 1983. On the field configuration in magnetic clouds. In: Solar Wind Conference. pp. 731.–733.

Gulisano, A. M., Dasso, S., Mandrini, C. H., Démoulin, P., 2005. Magnetic clouds: A statistical study of magnetic helicity. Jour. of Atmos. and Solar-Terrestrial Phys., 67, 1761–1766.

Gulisano, A. M., Dasso, S., Mandrini, C. H., Démoulin, P., 2007. Estimation of the bias of the minimum variance technique in the determination of magnetic clouds global quantities and orientation. Advances in Space Research.

Hidalgo, M. A., Cid, C., Vinas, A. F., Sequeiros, J., 2002. A non-force-free approach to the topology of magnetic clouds in the solar wind. Journal of Geophys. Res., 107 (A1), 1002.1–1002.7.

Hidalgo, M. A., 2003. A study of the expansion and distortion of the cross section of magnetic clouds in the interplanetary medium. Journal of Geophys. Res., 108 (A8), 1320.1–1320.6.

Hu, Q., Sonnerup, B. U. Ö., 2001. Reconstruction of magnetic flux ropes in the solar wind. Geophys. Res. Let., 28, 467–470.

Lepping, R. P., Burlaga, L. F., Jones, J. A., 1990. Magnetic field structure of interplanetary magnetic clouds at 1 AU. Journal of Geophys. Res., 95, 11957–11965.

Lepping, R. P., Acuna, M. H., Burlaga, L. F., Farrell, W. M., Slavin, J. A., Schatten, K. H., Mariani, F., Ness, N. F., Neubauer, F. M., Whang, Y. C., Byrnes, J. B., Kennon, R. S., Panetta, P. V., Scheifele, J., Worley, E. M., 1995. The Wind Magnetic Field Investigation. Space Science Reviews, 71, 207–229.

Lepping, R. P., Berdichevsky, D. B., Szabo, A., Arqueros, C., Lazarus, A. J., 2003. Profile of an Average Magnetic Cloud at 1 au for the Quiet Solar

Phase: Wind Observations. Solar Phys., 212, 425–444.

Lundquist, S., 1950. Magnetohydrostatic fields. *Ark. Fys.* 2, 361–365.

Luoni, M. L., Mandrini, C. H., Dasso, S., van Driel-Gesztelyi, L., Démoulin, P., 2005. Tracing magnetic helicity form the solar corona to the interplanetary space. Jour. of Atmos. and Solar-Terrestrial Phys., 67, 1734–1743.

Lynch, B. J., Zurbuchen, T. H., Fisk, L. A., Antiochos, S. K., 2003. Internal structure of magnetic clouds: Plasma and composition. Journal of Geophys. Res., 108 (A6), 1239.1–1239.14.

Mandrini, C. H., Dasso, S., Luoni, M. L., Pohjolainen, S., Démoulin, P., van Driel-Gesztelyi, L., 2005a. Quantitative Link Between Solar Ejecta and Interplanetary Magnetic Clouds: Magnetic Helicity. In: Innes, D. E., Lagg, A., Solanki, S. A. (Eds.), ESA SP-596: Chromospheric and Coronal Magnetic Fields.

Mandrini, C. H., Pohjolainen, S., Dasso, S., Green, L. M., Démoulin, P., van Driel-Gesztelyi, L., Copperwheat, C., Foley, C., 2005b. Interplanetary flux rope ejected from an X-ray bright point. The smallest magnetic cloud source-region ever observed. Astron. Astrophys., 434, 725.–740.

Mulligan, T., et al., 1999. In: Solar Wind Nine, AIP Conference Proceedings. Vol. 471. pp. 689–692.

Nakwacki, M. S., Dasso, S., Mandrini, C. H., Démoulin, P., 2005. Helicity analysis for expanding magnetic clouds: A case study. *Proc. Solar Wind 11 - SOHO 16, ESA* SP-592, 629–632.

Ogilvie, K. W., Chornay, D. J., Fritzenreiter, R. J., Hunsaker, F., Keller, J., Lobell, J., Miller, G., Scudder, J. D., Sittler, Jr., E. C., Torbert, R. B., Bodet, D., Needell, G., Lazarus, A. J., Steinberg, J. T., Tappan, J. H., Mavretic, A., Gergin, E., 1995. SWE, A Comprehensive Plasma Instrument for the Wind Spacecraft. Space Science Reviews, 71, 55–77.

Osherovich, V. A., Farrugia, C. J., Burlaga, L. F., 1993a. Nonlinear evolution of magnetic flux ropes. I - Low-beta limit. Journal of Geophys. Res., 98 (A8), 13225–13231.

Osherovich, V. A., Farrugia, C. J., Burlaga, L. F., Lepping, R. P., Fainberg, J., Stone, R. G., 1993b. Polytropic relationship in interplanetary magnetic clouds. Journal of Geophys. Res., 98 (A9), 15331–15342.

Riley, P., Linker, J. A., Lionello, R., Mikić, Z., Odstrcil, D., Hidalgo, M. A., Cid, C., Hu, Q., Lepping, R. P., Lynch, B. J., Rees, A., 2004. Fitting flux ropes to a global MHD solution: a comparison of techniques. Jour. of Atmos. and Solar-Terrestrial Phys., 66, 1321–1331.

Russell, C. T., Shinde, A. A., 2005. On Defining Interplanetary Coronal Mass Ejections from Fluid Parameters. Solar Phys., 229, 323–344.

Shimazu, H., Vandas, M., 2002. A self-similar solution of expanding cylindrical flux ropes for any polytropic index value. *Earth, Planets, and Space* 54, 783–790.

Sonnerup, B. U., Cahill, L. J., 1967. Magnetosphere structure and attitude from Explorer 12 observations. Journal of Geophys. Res., 72, 171–183.

van Driel-Gesztelyi, L., Démoulin, P., Mandrini, C. H., 2003. Observations of magnetic helicity. Adv. in Space Res., 32, 1855–1866.

Vandas, M., Romashets, E. P., 2002. In: Solar Variability: From Core to Outer Frontiers. Vol. ESA SP-506. pp. 217–220.

Webb, D. F., Lepping, R. P., Burlaga, L. F., DeForest, C. E., Larson, D. E., Martin, S. F., Plunkett, S. P., Rust, D. M., 2000. The origin and development of the May 1997 magnetic cloud. Journal of Geophys. Res., 105 (A14), 27251–27260.

Wimmer-Schweingruber, R. F., Crooker, N. U., Balogh, A., Bothmer, V., Forsyth, R. J., Gazis, P., Gosling, J. T., Horbury, T., Kilchenmann, A., Richardson, I. G., Richardson, J. D., Riley, P., Rodriguez, L., Steiger, R. V., Wurz, P., Zurbuchen, T. H., 2006. Understanding Interplanetary Coronal Mass Ejection Signatures. Space Science Reviews 123, 177–216.

Fig. 1. Magnetic cloud orientation. The directions of the GSE system (X, Y, Z, in the figure) are shown together with the ecliptic (horizontal in figure) plane. The magnetic cloud axis defines the angles θ and ϕ.

Table 1

General information for the clouds. Each row corresponds to a different cloud. The first column indicates the cloud number, the second and third columns show the initial and final times (day/month/year hh:mm, in Universal Time), respectively, the fourth and sixth columns correspond to the angles (θ and ϕ) that give the cloud axis orientation found by minimun variance analysis, the fifth and seventh columns show the angles (θ_l and ϕ_l) given in Lepping's web page (http://lepmfi.gsfc.nasa.gov/mfi/mag_cloud_S1.html), the eighth column is the mean value of the proton β parameter (β_p) during the MC observation, and the last column shows the impact parameter as informed in Lepping's web page.

Fig. 2. Proton β parameter (β_p) for the three studied MCs. Left panel corresponds to cloud 1, central panel to cloud 2, and right panel to cloud 3. The values derived from observations are shown with small dots. Vertical dashed lines indicate the MC boundaries (as given in Table 1). Horizontal dotted lines mark the reference value $\beta_p = 0.12$.

Table 2

Parameters derived from the bulk speed observations. The first column shows the cloud number (each row corresponds to a different MC), the second one T, and the third one the mean velocity. The fourth, fifth, and sixth columns correspond to the initial, static and final radii, respectively.

Fig. 3. The three velocity profiles. The left panel corresponds to cloud 1, the central one to cloud 2, and to right one to cloud 3. The observations are shown with dots and the fitting is indicated by a thick full line. The two vertical dashed lines mark the cloud start and end times.

Table 3

Fitted magnetic parameters. The first column corresponds to the cloud number and the second to the model (S for static Lundquist and E for self-similar expansion), the third, fourth and fifth columns are the fitted values (B_0 and α for S, and $\hat{B}_0$, $\hat{\alpha}$, and $\hat{t}$ for E), the last column shows the χ^2 values which indicate the qualitiy of the fitting. Notice that in model E, $\alpha(t)R(t) = \hat{\alpha}R_0(1 + \hat{t}/T)$ remains as a constant.

Fig. 4. Magnetic field profiles. Left, central, and right panels correspond to clouds 1, 2, and 3, respectively. The observations are shown with dots, S model is indicated by thick dashed lines, and E model by thin full lines. Vertical thin dashed lines mark the start, center and end times for each MC (see main text).

Table 4

Global MHD quantities for the fitted models. The first column indicates the cloud number, the second one the model (S for static Lundquist and E for self-similar expansion), the next five columns show the global quantities in the following order: the magnetic flux across a surface perpendicular to $\hat{z}_{cloud}$, the magnetic flux per unit length across a surface perpendicular to $\hat{y}_{cloud}$ (which is similar to $\hat{\phi}$ for a low impact parameter as in the clouds studied here, see Sec. 3.1), the magnetic helicity per unit length (Eqs. (6) and (20)), and the initial and final magnetic energy per unit length.

Fig. 1.

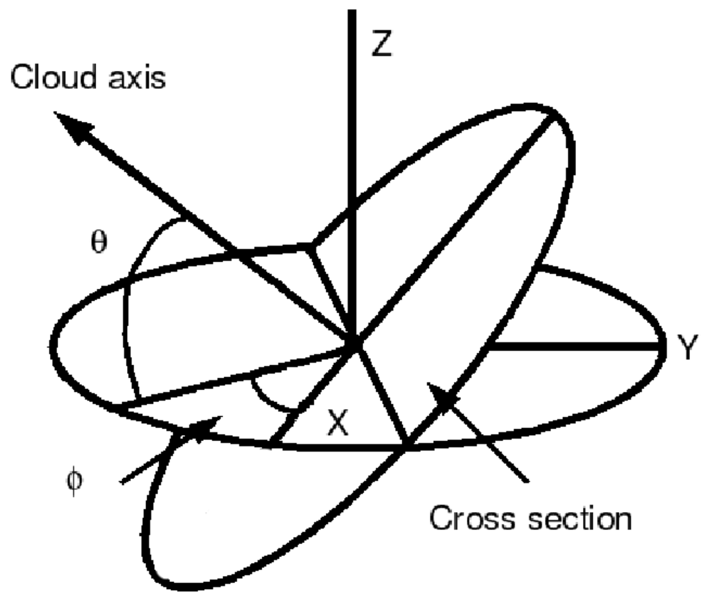

Table 1

MC	Start	End	θ	θ_l	ϕ	ϕ_l	$< \beta_p >$	p_l
1	20/08/98 10:18	21/08/98 19:18	14°	18°	294°	287°	0.045	-13 %
2	09/08/99 10:48	10/08/99 15:48	75°	75°	138°	133°	0.072	26%
3	22/04/01 00:54	23/04/01 01:24	−62°	−78°	274°	293°	0.074	5%

Fig. 2.

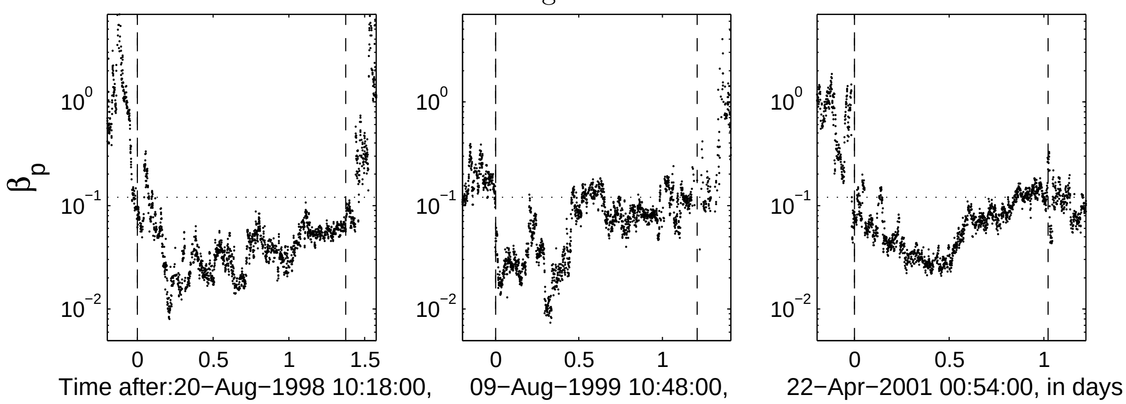

Table 2

MC	T	$< V_{x,cloud} >$	R_0	R_s	R_f
	(days)	(km/s)	(AU)	(AU)	(AU)
1	9.2	-256	0.09	0.10	0.11
2	8.6	-315	0.10	0.11	0.12
3	6.1	-357	0.09	0.10	0.11

Fig. 3.

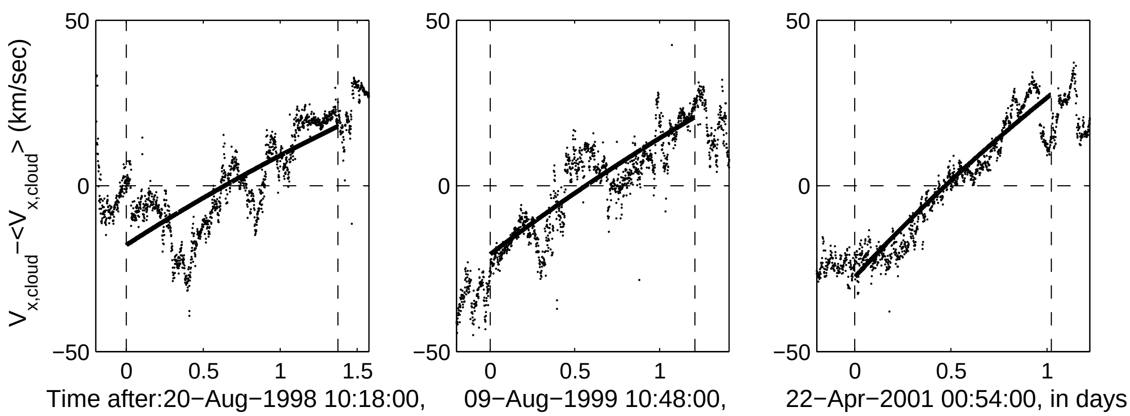

Table 3

MC	Model	B_0 or $\hat{B}_0$ (nT)	α or $\hat{\alpha}$ (AU^{-1})	$\hat{t}$ (days)	χ^2 (nT^2)
1	S	16	28	–	25
1	E	33	43	-3	14.4
2	S	11	-19	–	20.3
2	E	20	-25	-2.4	20.3
3	S	14	-20	–	10.9
3	E	18	-23	-0.4	6.8

Table 4

MC	Model	Φ_z $nTAU^2$	Φ_ϕ/L nTAU	H_r/L nT^2AU^3	E_m^0/L nT^2AU^2	E_m^f/L nT^2AU^2
1	S	0.15	0.70	0.15	0.15	-
1	E	0.13	0.90	0.17	0.20	0.19
2	S	0.21	0.45	-0.11	0.10	-
2	E	0.21	0.54	-0.13	0.12	0.11
3	S	0.26	0.57	-0.17	0.16	-
3	E	0.25	0.63	-0.18	0.18	0.16

Fig. 4.

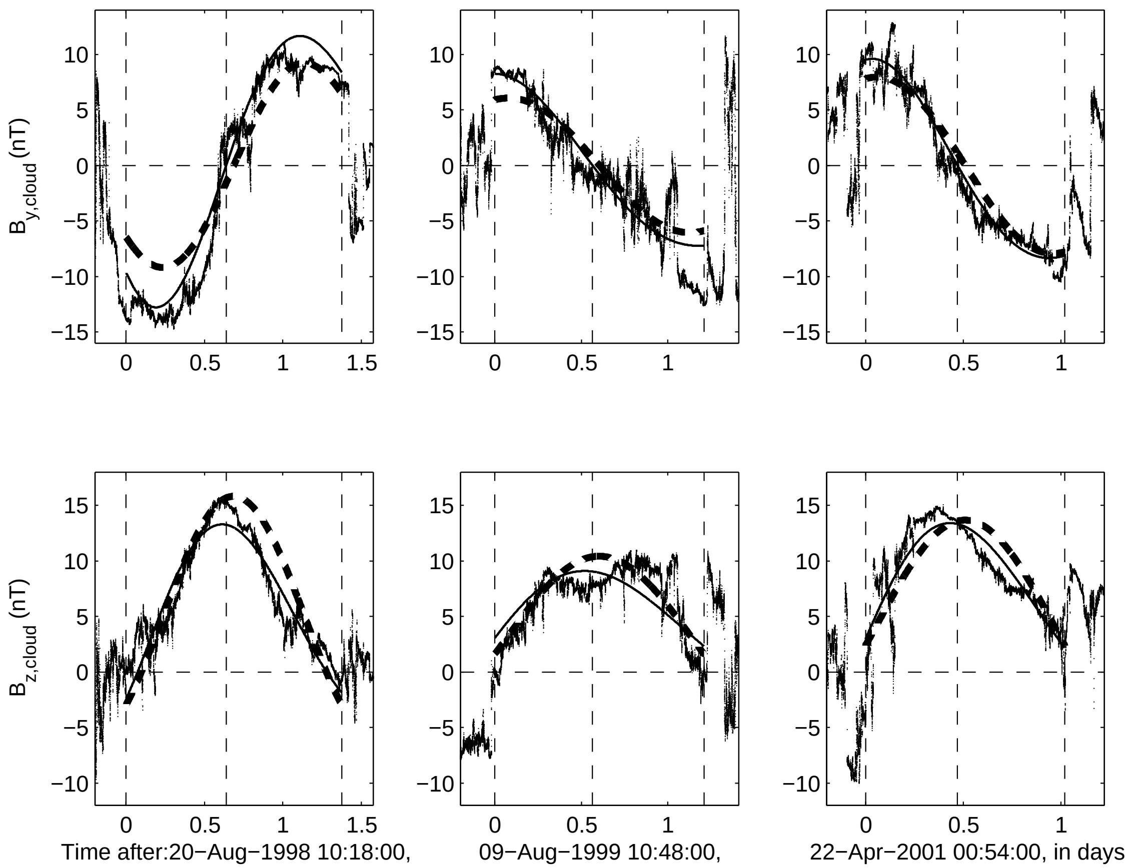
B_{y,cloud} (nT)
B_{z,cloud} (nT)
Time after:20−Aug−1998 10:18:00,
09−Aug−1999 10:48:00,
22−Apr−2001 00:54:00, in days